CrossMark

A generic platform for hyperspectral mapping of wood

Nele Defoirdt[1,2] · Ali Sen[3] · Jelle Dhaene[2,4] ·
Tom De Mil[1,2] · Helena Pereira[3] · Joris Van Acker[1,2] ·
Jan Van den Bulcke[1,2]

Abstract Sustainable use is essential to guarantee future availability of wood. Structural and chemical mapping can contribute to fit-for-purpose usage, as accurate and detailed knowledge of the material enables guided utilization and optimal performance of wood. The platform presented in this paper, illustrated on poplar disks for early selection, collects data in the NIR, visual and X-ray spectrum in maximum 30 min per wood disk. Flatbed scanning proves to be a cheap and fast technique to evaluate basic physical properties such as cross-sectional area and wood density. X-ray CT scanning is used for density mapping adding information on density variation between and within disks. Chemometric modeling of infrared spectra is used to map density, tension wood and lignin content. X-ray- and NIR-based density mapping showed good correlation, although NIR-based maps do not show the same level of detail as X-ray images do due to lower resolution. Results of NIR-based hyperspectral mapping illustrate that tension wood zones were denser and contained less lignin which corresponds with the existence of the G-layer described in the literature. In all, the combination of high-end tools together with simple tools such as flatbed scanning allows for high-throughput and high-resolution quantitative mapping of some of the main properties of poplar wood. Furthermore, infrared scanning can be used to map density, tension wood and chemistry without

✉ Nele Defoirdt
  Nele.Defoirdt@UGent.be

[1] Woodlab-UGent, Department of Forest and Water Management, Faculty of Bioscience Engineering, Ghent University, Coupure Links 653, 9000 Ghent, Belgium

[2] UGCT, University Ghent Centre for X-ray Tomography, Proeftuinstraat 86, 9000 Ghent, Belgium

[3] Centro de Estudos Florestais, Instituto Superior de Agronomia, Universidade de Lisboa, Tapada da Ajuda, 1349-017 Lisbon, Portugal

[4] Department of Physics and Astronomy, Institute for Nuclear Sciences, Ghent University, Proeftuinstraat 86, 9000 Ghent, Belgium

the need for more complex, expensive and/or time-consuming methods, yet with less accuracy and lower resolution, thus being applicable as single tool for breeding selection.

Introduction

Globally more than 3.5 billion m^3 of wood is harvested each year (FAOSTAT 2013). With an increasing world population, an increasing standard of living and the emergence of a bio-based economy relying on a lignocellulosic biomass backbone, wood consumption will increase correspondingly, especially taking into account the current interest in biofuels (Grayson 2011). To guarantee wood supply as a source of biomass, timber, paper, fuel and biomaterials, the sustainable management of forests and plantations and an acceleration of forest domestication are essential (Harfouche et al. 2012). Proper optimization of the forestry-wood chain is based on feedback between tree breeders, biotechnologists, foresters, wood technologists and the wood processing industry, to focus on traits that improve productivity, sustainability and wood quality.

Detailed mapping of wood properties and associated variability helps to adapt breeding and forest management strategies related to the envisaged end-product and enables the exploitation of the full potential of purpose-grown trees, optimizing the use of local-grown material and as such increase self-sufficiency. Trees can be grown for use as timber for construction or engineered wood products and wood-based panels, requiring wood with certain mechanical properties exhibiting low variability, or for fiber-based products, for example pulp for paper, for which a different set of properties, mainly chemically, is targeted. There is a need for mapping wood density and composition of transgenic trees with reduced lignin, modified lignin, or increased cellulose and hemicellulose guiding breeders toward maximum yield and optimization, and/or to steered control of thermal conversion of biomass (Bahng et al. 2009), for biofuel and value-added biochemical production. For instance in thermochemical or gasification approaches, increased density will be an important trait, while increased lignin content might be a desired trait for direct firing or co-firing of wood for energy (Hinchee et al. 2009). For bioethanol production from lignocellulosic biofuel crops, the recalcitrant complex formed by the main cell wall components of wood hinders easy and low-cost accessibility to the structural sugar polymers (Wyman 2007; Brereton et al. 2012). Therefore, the final glucose yields can be improved by inducing tension wood without a detrimental impact on biomass yield (Brereton et al. 2011). Tension wood has gelatinous fibers that have a barely lignified thickened layer at the inside of the secondary cell wall, commonly known as the G-layer that contains up to 20% more cellulose (Timell 1969). Quantification and mapping are also of importance from an ecophysiological point of view. For instance, lignins, constituting about 20–30% of the dry wood mass (Boerjan et al. 2003), play a role in mechanical rigidity, water repellence, chemical resistance and with that the defense system of the tree (Polle et al. 1997; Whetten et al. 1998). A number of studies concluded that the chemical composition of woody plants varies greatly across different parts of the plant

anatomy and is highly influenced by a variety of genetic and environmental factors (McKendry 2002; Hou and Li 2011). Such studies may profit from high-throughput measurement techniques that allow large sampling sizes as required for statistical analysis.

The above-mentioned examples show that there is a clear need for the development of a platform or tool chain for high-resolution and high-throughput mapping of wood properties. Currently, equipment such as Silviscan enables to determine within-tree distribution of wood properties (Defo et al. 2009), density and anatomical properties (Vahey et al. 2007; Zhu et al. 2007) on wood strips. The platform proposed here also works toward an integration of different wavelength-based systems, focusing on wood disks for fast structural and chemical characterization of wood, and visualization and quantification of within-tree variability in either 2D or 3D. The main techniques that are part of this tool chain are flatbed scanning, helical X-ray computed tomography (X-ray CT) and near-infrared (NIR) hyperspectral imaging.

Flatbed scanning in combination with image processing generates general data such as cross-sectional area and shape, and amount of bark, thereby providing a very straightforward and cheap technique that is generally applicable. X-ray CT is gaining significant interest, and its multi-purpose use is widely recognized in wood science and technology, especially for structural analysis (i.a. Van den Bulcke et al. 2008; Mayo et al. 2010). The technique is well suited for studying wood density in three dimensions (Freyburger et al. 2009; Skog and Oja 2009), which is of importance since density is considered a key variable for understanding tree structure and is relevant for timber properties including the energy content (De Ridder et al. 2011; Van den Bulcke et al. 2013). NIR spectroscopy is also widely used in many research fields, mostly to derive material characteristics such as chemical information from the object under study. This technique, next to fluorescence spectroscopy (Nkansah and Dawson-Andoh 2010a, b), is an alternative for the time-consuming, labor-intensive, expensive and destructive conventional wet chemical analytical methods (Williams 2009; Nkansah and Dawson-Andoh 2010a; Hou and Li 2011; Riddell et al. 2012). Application of NIR spectroscopy has been elaborated on in recent years, for example on solid wood (Schimleck et al. 2002; Kelley et al. 2004; Jones et al. 2006; Poke and Raymond 2006), ground wood (Raymond and Schimleck 2002; Hou and Li 2011) as well as pulps (Santos et al. 2014, 2015) when properly calibrated. Recent progress of this technology allows high-resolution near-infrared hyperspectral image acquisition, resulting in an infrared spectrum for each pixel of the image. An overview of recent near-infrared research for wood and paper is given by Tsuchikawa (2007), Tsuchikawa and Schwanninger (2013) and Tsuchikawa and Kobori (2015), while So et al. (2004) also introduced many systematical articles and explained that the rapid assessment of solid wood properties using NIR spectra is a fast-growing field that has broad implications in relation to wood quality and, ultimately, tree improvement.

The tool chain is illustrated on small poplar (*Populus* spp.) wood disks. This tree species is studied intensively given its fast growth potential, capacity to be grown in coppicing systems and it is amenable to genetic modification (Zhou et al. 2011; Aylott et al. 2008; Rae et al. 2009). Furthermore, coloring methods and/or the variation in shiny appearance allows visualization of tension wood zones (Ritter

et al. 1993; Badia et al. 2005), thereby having a structural and chemical variability which can be used for modeling as well as model validation. It is illustrated that flatbed, X-ray CT and NIR scanning are complementary imaging modalities for mapping wood properties. Furthermore, the use of NIR hyperspectral imagery as proxy for density and lignin content determined using analytical pyrolysis as well as tension wood is exemplified.

Materials and methods

Figure 1 gives a schematic overview of sample preparation of the different disks and their respective use.
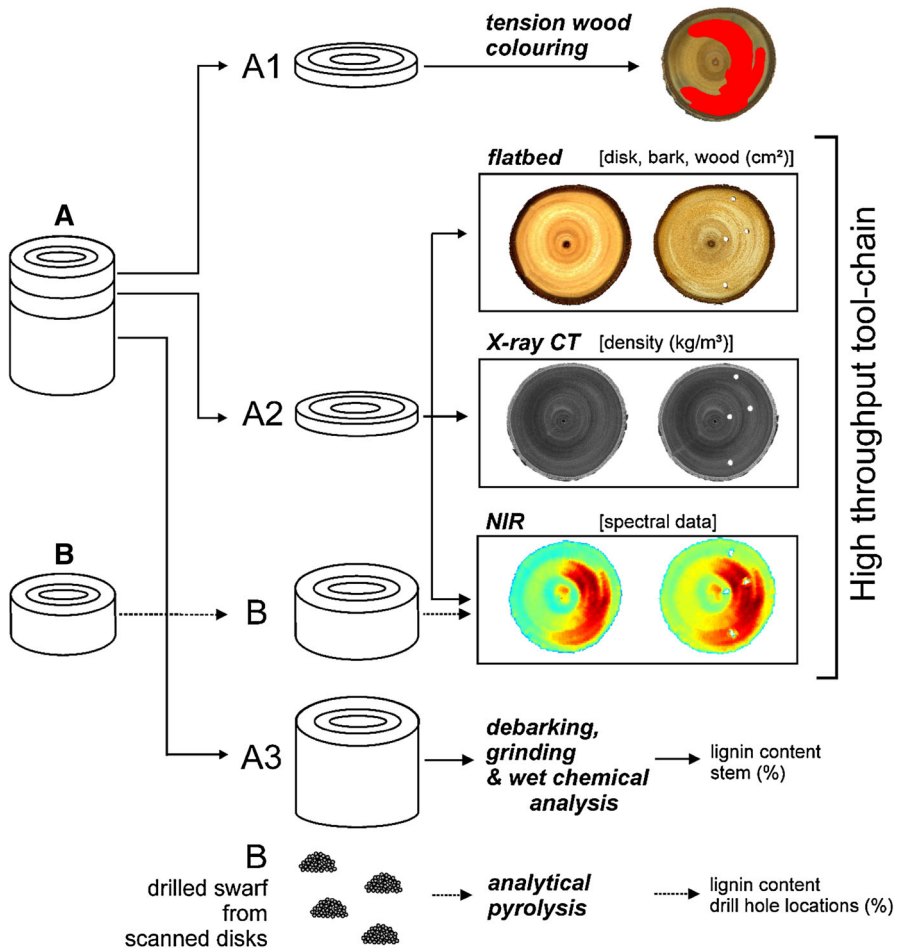
Fig. 1 Data collection scheme for sample sets A and B

Ten four-year-old poplar stems from *Populus x canadensis* "Tardif de Champagne" (sample set A) were selected from an experiment for inducing tension wood formation by tilting young trees grown in containers. They are therefore exemplary for illustrating the potential of property mapping by the tool chain revealing within-disk differences in tension wood, density and lignin content. Stem diameters ranged from 30 to 80 mm. Three adjacent disks: two with an approximate thickness of 5 mm (A1 and A2) and one with an approximate thickness of 50 mm (A3), were sawn from each stem and stored in a refrigerator, resulting in three matching sets of 10 disks.

A second set (B) of 29 two-year-old poplar stems from *P. x canadensis* "Muur," *P.* x *canadensis* "Oudenberg," *P.* x *canadensis* "Vesten," *P. maximowiczii* x *P. trichocarpa* "Bakan," *P. maximowiczii* x *P. trichocarpa* "Skado," *P. deltoides x* (*P. trichocarpa* x *P. deltoides*) "Grimminge" from a short rotation experiment were sampled and used for the development of lignin and tension wood models. Diameters ranged from 30 to 80 mm. From each stem, a 25-mm-thick disk was sawn and stored in a refrigerator (set B).

Tension wood coloring

On the wood disks of set A1, tension wood was identified using a standard coloring method with a ½ diluted zinc-chloro-iodine solution similar to the Schulze's solution, more specifically a mixture of 1 mL iodine solution (1 g I_2 + 10 g KI dissolved in 37.5 mL H_2O) and 30 mL saturated $ZnCl_2$ solution (i.e., 4320 g L^{-1} at 25 °C). When this solution is brushed on freshly sawn stem disks, normal wood turns light yellow to brown, whereas tension wood colors dark brown to orange because of its higher cellulose content. The tension wood zones are then marked with persistent ink. The second set of disks (A2) was used as verification of tension wood zones based on the visible difference in shininess, since Badia et al. (2005) found that tension wood coloring was not always as effective as required. For set B, tension wood zones were only visually distinguished.

State-of-the-art tool chain

The disks of set A2 were used for the development of the NIR model for density and to illustrate the tool chain, whereas the disks of set B were used for the development of the NIR models for tension wood and lignin content. Holes were drilled at preselected locations both in the A2 and B disks, and only the wood properties from those drilled locations were used for model building. Selective drilling in normal or tension wood provided binary tension wood data (0 = normal wood, 1 = tension wood) for all drill hole locations. The lignin content of the drill holes of disks B was determined by analytical pyrolysis of the drilled swarf. The analytical pyrolysis was performed at the Centro de Estudos Florestais of the Universidade de Lisbon (Portugal) according to Alves et al. (2011). As described there, each sample (75–80 μg) was pyrolyzed at 600 °C for 5 s. Pyrolysis lignin was determined based on the identification of pyrolysis products from previous in-house research. Finally, all disks of set A2 were scanned with the tool chain before and after drilling the

holes, whereas disks of set B were only scanned with the NIR setup. The coordinates of the holes determined on the scans after drilling were used to extract the data from the images taken before drilling. As such, on one and the same disk, data on tension wood classification, lignin content, X-ray CT-derived density (cfr. "Helical X-ray CT (HXCT)" section) and the NIR spectra (cfr. "Near-infrared (NIR) hyperspectral imaging" section) were collected for each of the drill hole locations and this information was used for NIR model building.

Flatbed scanning

The freshly cut samples of set A2 were weighed to the nearest 0.0001 g using a Sartorius precision balance. The disks were scanned with an Epson Perfection 4990 Photo flatbed scanner at 508 dpi, resulting in a pixel size of approximately 50 µm. Semiautomated analysis of the images in MATLAB® resulted in the cross-sectional area of the disk, which was used for calculation of the green volume, i.e., the volume of the samples when the tree was freshly cut. The area and proportion of the bark and wood were also obtained. Subsequently, the disks were dried for 24 h at 103 °C and weighed again. Moisture content (%) and basic density (kg m^{-3}), which is the oven-dry mass of a wood sample divided by its green volume, were calculated.

Helical X-ray CT (HXCT)

The scanner used here, further referred to as Nanowood, is a setup developed at UGCT, the Ghent University Centre for X-ray Tomography (www.ugct.ugent.be) in collaboration with the company X-ray Engineering (XRE; www.xre.be). The scanner has a generic in-house developed CT scanner control software platform (Dierick et al. 2010) that allows full control of the scanner hardware. A detailed description and performance assessment of Nanowood can be found in Dierick et al. (2014). All oven-dried disks of set A2 were mounted in a custom-made sample holder and scanned using the helical X-ray CT setup. Scans were performed with an average voltage of 90 kV using a 0.45-mm aluminum filter. Reconstruction was performed with Octopus, a tomography reconstruction package for parallel, cone-beam and helical geometry (Vlassenbroeck et al. 2007), currently licensed by InsideMatters (www.insidematters.eu). The data volume was reconstructed with the helical Katsevich algorithm implemented on GPU. As such, the 16-bit grayscale volumes of the 10 disks were available with an approximate voxel pitch of 60-µm resolution. Each disk volume was extracted from the stack using Octopus Analysis, also licensed by InsideMatters, formerly known as Morpho + (Brabant et al. 2011), a software package for volume analysis. Subsequently, the 16-bit grayscale values of the reconstructed disks were converted to absolute densities in MATLAB®. The conversion procedure can be found in De Ridder et al. (2011). Density in axial direction was averaged resulting in a 2D density map of each disk. A cross-sectional view through the stack of disks is illustrated in Fig. 2. Bark has a higher ash and mineral content compared to wood (Tharakan et al. 2003; Mézáros et al. 2004), which results in a different attenuation. Therefore, bark shown in the disk reconstructions only serves as demarcation, and density values of bark are as such not taken into account.
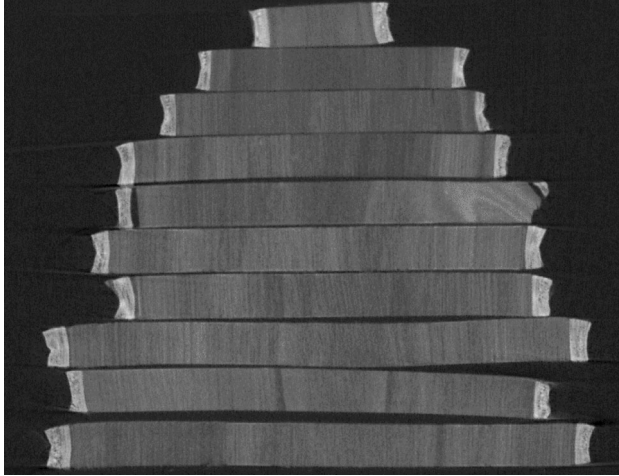
Fig. 2 Cross section through the entire X-ray CT stack from set A2

Near-infrared (NIR) hyperspectral imaging

Hardware setup The custom-made setup for infrared imaging is schematized in Fig. 3 and has the following components: stepper motor and drive (1), movable stage with sample (2), light source consisting of tunable quartz tungsten halogen lamps (3), lens (4), spectrograph (5), sensor (6) and computer (7).

The infrared line camera consists of an imaging spectrograph and detector for full spectral information ranging from 800 to 2500 nm. The quartz tungsten halogen
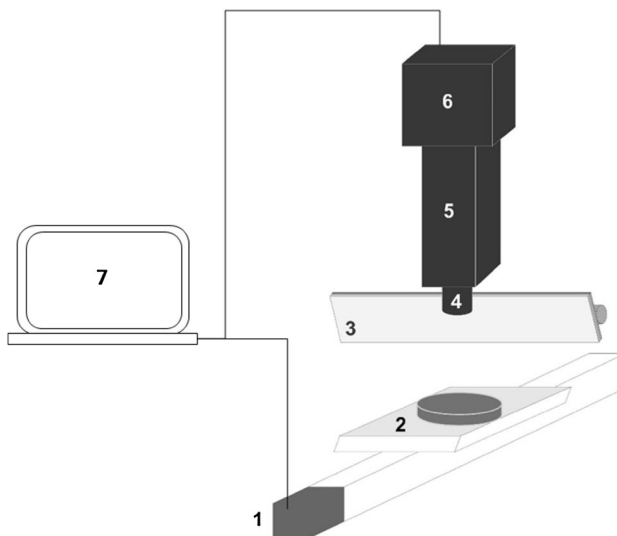
Fig. 3 Schematic overview of the NIR scanner

lamps are connected with a 12 V variable DC power supply. The light is focused by the lens through a small slit, through the spectrograph and onto the sensor. A spatial line is obtained with each scan, and the obtained image is an array of 320 pixels spatially and 256 pixels spectrally. The spatial resolution in this setup was 0.5 mm, whereas the width of one of the 256 wavelength bands was 6.64 nm.

Hardware control, i.e., camera control and sample translation, was implemented in the LabView software platform which is also used as the interface for the X-ray tomography scanner mentioned before (see Dierick et al. 2010). Acquisition was scripted, automating synchronization of image acquisition and sample movement.

The sample was moved automatically with a 0.5 mm step size. The exposure time for each image was 6 ms, and 50 frames were averaged for a single line. This resulted in a total of 60 up to 160 line scans for a full scan of one disk. Each sample as such consists of a three-dimensional volume, the third axis being the spectral dimension ranging from 800 to 2500 nm. All samples were sanded to minimize scattering due to surface roughness. The visible difference in shininess between tension wood and normal wood disappeared on the sanded surface of the disks, while at the other side of the disk, the shininess could be used to verify the tension wood coloring.

Preprocessing All processing was implemented in MATLAB$^{®}$. The following preprocessing steps are included: transformation to correct for lens distortions, normalization and transformation to absorbance values, noise filtering using a dedicated spot filter and light intensity correction. Lens distortions were corrected by imaging a grid of squares and calculation of the transformation matrix, which is then applied to all images. This is a scan-independent but device-/lens-dependent step and thus has only to be performed once. Normalization involved scanning a dark image (I_d) with the light switched off and a flat image of pure Teflon (I_f), used as reference material. The position of the Teflon reference board was adjusted such that its height was the same as the sample (Li et al. 2012). As such, all images (I) were normalized (I_n) and transformed to absorbance values using the following formula:

$$I_n = -\log_{10}\left(\frac{I - I_d}{I_f - I_d}\right) \tag{1}$$

In addition to the latter ad hoc intensity control, post hoc corrections were performed by including a reference material in the field of view at all times during scanning. Any light intensity fluctuations or possible heating was then corrected for by using the hyperspectral information of the reference material. A standard preprocessing procedure to correct for non-chemical biases such as inhomogeneous sample surface (Gowen et al. 2007) was implemented, including detrending, mean centering and taking the first derivative with Savitzky–Golay algorithm or the second derivative to remove baseline-offset (Schimleck et al. 2001; Fujimoto et al. 2010). The outermost wavelength bands of the spectra were clipped because of the lower sensor sensitivity at the extremes of the spectrum (see Arngren 2011).

Analysis   All analysis steps were implemented in MATLAB® and are schematically summarized in Fig. 4. NIR hyperspectral disk images were segmented from their background by using a magic wand tool-like function that groups pixels with a similar tone and color. The NIR images of the same disk before and after drilling were accurately aligned using a rigid body transformation. The same procedure was used for aligning the X-ray images of the same disk before and after drilling of the holes. The coordinates of the drill holes were used to extract data on exactly the same locations from the images before drilling. The NIR spectra of those locations could then be linked to the average X-ray-based density, the binary tension wood data as determined visually on the set B wood disks (0 = normal wood, 1 = tension wood) and the lignin content determined on the drill swarfs for those specific drill locations.

Based on aforementioned dataset, models could be built for density, tension wood and lignin content mapping using NIR images. The density model was built based on the pixel spectra and density results from the 20 drill locations of 5 disks of set A2. The tension wood and lignin models were built based on the pixel spectra and binary tension wood classification and lignin content data of 60 drill locations of 20 disks of set B. The dataset is therefore divided in a calibration (66%) and validation (34%) group. Using standard chemometrics, models were built for the three properties. An automated iterative partial least squares (PLS) model building
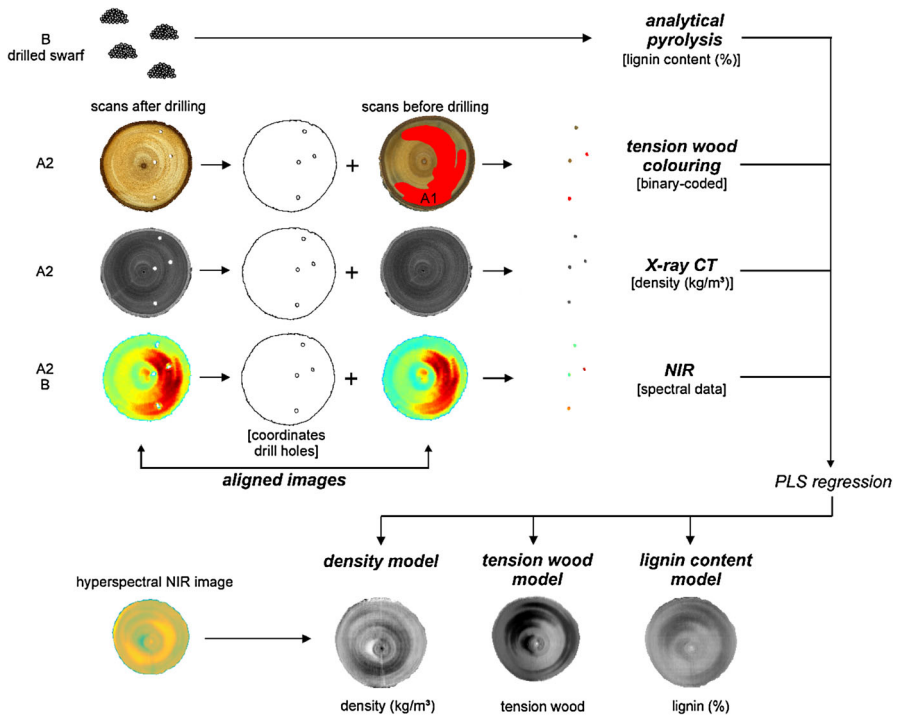
Fig. 4 Extraction of calibration data for model building and model application
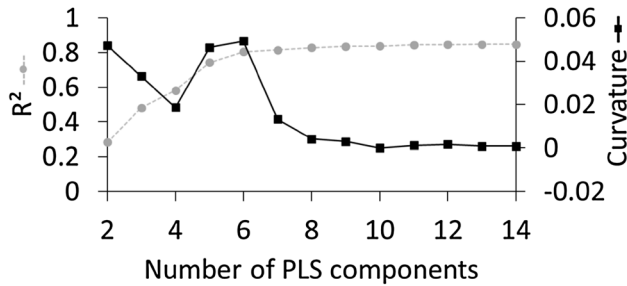
Fig. 5 R^2 and its curvature as a function of the number of model components in the lignin model

script, with 30 cross-validation steps per PLS run, was used to determine the amount of model components in an objective way. When plotted against R^2, maximal curvature, determined via gradient calculation, was used as criterion. Figure 5 illustrates this for the lignin model building. For the lignin model, the wavelength bands 165 up to 186 (ca. 1889–2035 nm), attributed to water (Schwanninger et al. 2011), were removed.

An extensive set of statistical measures, as listed in Hein et al. (2011) and suggested by Fujimoto et al. (2008) and Jones et al. (2006) compares models' calibration and validation. The quality of the final models in this platform is expressed as the coefficient of determination (R^2) and root-mean-squared error (RMSE) of the fitted versus observed data for the calibration as well as the validation dataset. Additionally, an extra validation test was run for the lignin and tension wood model for the nine disks of set B that were not used for model building. Lignin and tension wood models were applied using the NIR spectra of the 27 drill holes of those nine disks, and an average value for each drill hole was calculated.

Final models were applied to the NIR images of the 10 four-year-old disks of set A2 to illustrate the potential of the NIR technique to visualize variability within and between disks.

Lignin determination by chemical summative wet analysis

The disks of set A3 were used for chemical summative wet analysis including determination of Klason and acid-soluble lignin contents. Therefore, all material was debarked, ground and dried at 60 °C overnight and 100 °C for two hours before the analyses. For each disk, two replicates were run determining the average lignin contents of the stems of set A.

Klason and acid-soluble lignin contents were determined on material previously extracted by three successive Soxtec extractions with 110 mL of dichloromethane, ethanol and water for 1.5 h with each solvent using 2.0 g of wood. 3.0 mL H_2SO_4 (72%) was added to 0.35 g of extracted sample, and the mixture was placed in a water bath at 30 °C for 1 h, after which the sample was diluted to a concentration of 4% H_2SO_4 and hydrolyzed for 1 h at 120 °C and at 1.2 kg cm^{-2} pressure. The sample was filtered under vacuum through a glass filter crucible (G3) and washed

with ultra-pure (Milli-Q) water. Acid-soluble lignin was determined on the combined filtrate by measuring the absorbance at 206 nm using a Shimadzu UV-160A UV–Vis spectrophotometer. Klason lignin was determined as the mass of residue after drying at 100 °C. Measurements were reported as a mass percentage of the original sample, and Klason lignin and acid-soluble lignin contents were combined to obtain the total lignin content.

Results

Physical characteristics obtained via processing of the images of flatbed scanning and differential weighing of the disks of set A2 are listed in Table 1. Pyrolysis lignin values varied between 13.0 and 26.1% with an average of 21.9%. A significant difference (Student's t test, $p = 0$) in lignin content between tension wood and normal wood was found (Fig. 6).

The results of the tool chain are illustrated in Fig. 7. Details of the final models are listed in Table 2 and Fig. 8. The R^2 and RMSE of the independent validation sample set for lignin were 0.88 and 1.28%, respectively. The fitted versus observed values for that model are added in Fig. 8. When applying the tension wood model to the independent sample set, 24 of the 27 drill locations (i.e., 89%) were correctly classified as tension or normal wood. Two misclassified regions concerned small tension wood zones and probably contained both tension and normal wood.

Table 3 contains the lignin content of the 10 stems from set A, on the one hand determined by wet chemical analysis on disk set A3 and on the other hand calculated as the average value of the NIR modeled disk reconstructions excluding bark pixels from set A2.

Table 1 Physical characteristics of the wood disks of set A2

Disk ID	Cross-sectional area (cm^2)	Bark portion (vol%)	Green MC[a] (%)	Basic density (kg m^{-3})
1	8.50	17.5	144	420
2	12.93	15.1	158	400
3	18.77	14.3	160	410
4	23.84	13.2	158	450
5	24.74	16.2	129	450
6	30.13	15.5	107	490
7	30.34	19.8	138	460
8	37.41	13.3	141	470
9	44.60	13.9	116	470
10	45.70	17.4	129	480
Average	27.70	15.6	138	450
SD	12.50	2.1	18	31

[a] MC of freshly cut wood

**Fig. 6** Lignin content for tension wood and normal wood samples determined using analytical pyrolysis
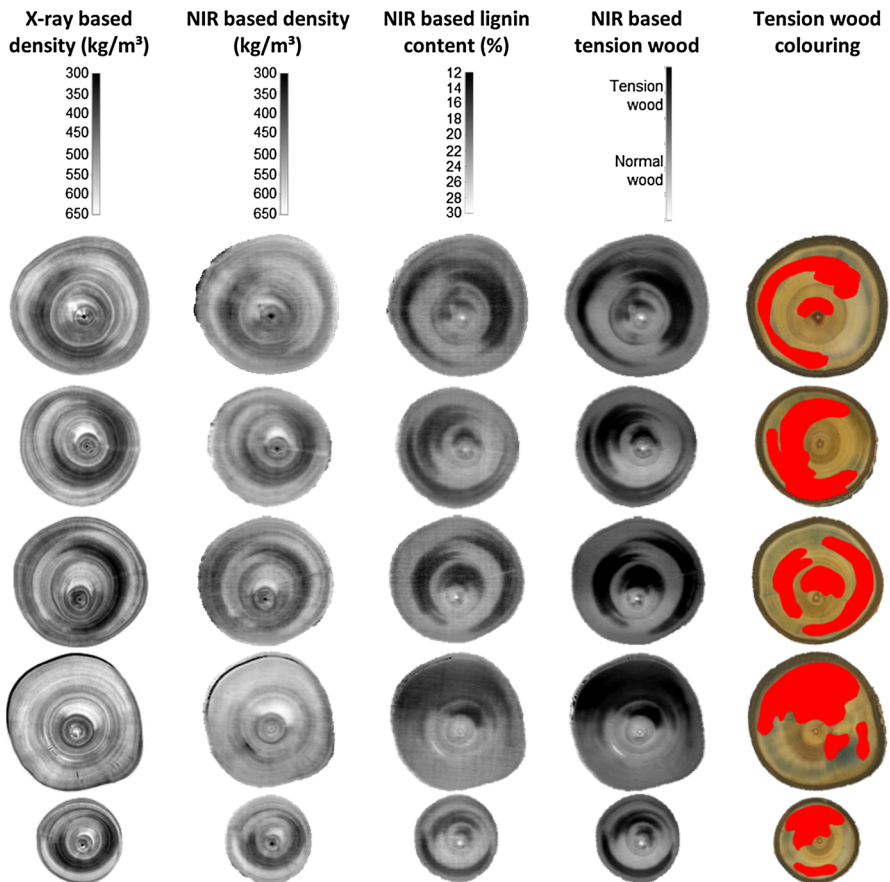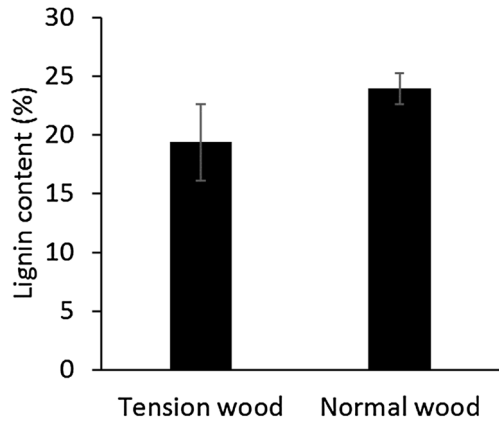
Fig. 7 Density mapping-based on X-ray imaging; density mapping, lignin content and tension wood mapping based on NIR scanning and tension wood coloring scans for five out of 10 disks

Table 2 Details of the PLS models using NIR data to map density, chemical composition and tension wood

	Density	Lignin	Tension wood
Sample set	A2	B	B
Number of disks/total drilled holes	5/20	20/60	20/60
Number of pixels[a]	336	563	563
Used derivative from the NIR spectra	Second	Second	First with Savitzky–Golay
Wavelength bands	15–220	30–155, 188–221	15–220
Number of components	4	6	4
R^2 (cross-validated) calibration data	0.87	0.81	0.64
RMSE (cross-validated) calibration data	19.54 kg m^{-3}	1.12%	0.28
R^2 validation data	0.90	0.79	0.60
RMSE validation data	17.46 kg m^{-3}	1.18%	0.28

[a] 66% of the data is used for model calibration, 34% of the data for model validation
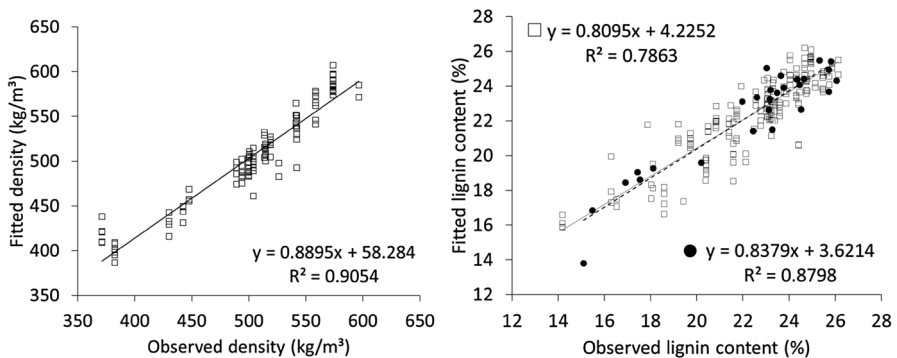
Fig. 8 Fitted versus observed values of the validation set for density (*left*) and lignin (*right*, *squares* for the validation set, *black filled circles* for the independent validation set)

Discussion

The different components of the tool chain described in this paper vary in complexity as well as output. Flatbed scanning is a fast and cheap technique to obtain accurate details on the shape and size of wood disks, particularly interesting for irregularly shaped samples. Bark, heartwood and pith area can be computed using image analysis, as well as shape-related parameters, and when including wet and dry mass and thickness measurements, basic density and green moisture content are easily calculated (Verlinden et al. 2013; Wassenberg et al. 2014; Hackenberg et al. 2015). One can also use the information in the optical range of the spectrum, thus to obtain device-independent color properties of the wood surface once calibrated properly (i.a. León et al. 2006). Headlee et al. (2013) concluded that basic

Table 3 Lignin content of the poplar samples in % of the oven-dry mass determined by wet chemical analysis (average of two replicates) and NIRS

	Disk ID	1	2	3	4	5	6	7	8	9	10
Wet chemical analysis	Lignin	23.79	23.79	22.39	20.76	19.60	19.55	20.62	20.45	20.34	19.53
	Klason	20.43	20.47	18.79	18.30	17.43	18.39	17.99	18.75	18.98	16.43
	Acid soluble	3.36	3.32	3.60	2.46	2.17	1.16	2.63	1.70	1.36	3.10
NIRS	Lignin	19.25	19.59	18.34	18.21	19.99	19.39	18.77	18.63	18.72	18.49

density is influenced by the within-tree position, genotype × environment interactions and taxonomic sections, species and genomic groups, and thus a high-throughput method for measuring wood density is necessary i.a. for poplar breeding studies. When high-throughput analysis of the tool chain is envisaged, at least 30 disks an hour can be scanned and analyzed. Use of a digital camera and integration in the NIR setup could be an option as well, especially for larger stem disks, similar to the approach for wood cores and stems employed by the LignoStation[TM] system of Rinntech[®]. It can be noted that green moisture contents measured in this study are in the ranges reported by Kenney et al. (1990). The density data of the sample set in this study concurs too with that of other studies (Murphey et al. 1979; Blankenhorn et al. 1992; Geyer et al. 2000; Semen et al. 2001; Headlee et al. 2013). The bark portion is mostly reported as mass percentage (i.a. Guidi et al. 2008; Tharakan et al. 2003), but determining the volumetric bark content on images of the fresh disks is simpler and faster as physically separating bark from wood is avoided.

X-ray CT scanning results in detailed information on the 3D density distribution of wood (i.a. De Ridder et al. 2011; Li et al. 2013). Helical scanning enables high-resolution scans of an entire stack of disks without the artifacts of standard cone-beam tomography. When using the same setup and settings as mentioned in this paper, a total of 30 disks (0.5 cm thickness) can be scanned at once within approximately 1 h. Other techniques, either based on high-frequency or X-ray scanning (Schinker et al. 2003), such as LignoStation[TM] (developed by Rinntech[®]) and Silviscan, respectively, are able to scan wood strips or disks to a certain extent, but are limited to 2D. The same physical parameters can be calculated as obtained from flatbed scans, but the equipment is more expensive, still less available, and trained operators are needed, although due to its increased use, availability and user-friendly usage are increasing. The entire platform presented in this paper is not yet used for cores, but future adaptations for that purpose seem interesting and are already in place for X-ray CT scanning aiming at tree ring analysis (Van den Bulcke et al. 2014; De Mil et al. 2016).

Both flatbed and X-ray CT scanning do not directly relate to the chemical composition of the disks. Although wet chemistry is still the pre-eminent technique for chemical quantification, cost of analysis, both in terms of man power and time and limited use when only smaller sample sizes are available, stresses the need for other techniques such as NIR scanning. The alignment procedure presented in this paper allows for extraction of different types of data from different imaging

modalities at exactly the same locations as for calibration of the models. Meder et al. (2010) have also reported on the use of a custom-built spatially resolved NIR scanner for tree increment cores, while Mora et al. (2011) and Thumm et al. (2010) reported on a system for scanning disks with a NIR camera to acquire a 2D mapping of the chemical composition of *Pinus radiata*. Thumm et al. (2010) mentioned the disk was seemingly composed of two separate halves, due to the rotational movement implemented in their setup. A rotational movement is also possible in the present system but, especially for smaller disks, a translation is beneficial and is used here, as such avoiding aforementioned artifact. The NIR scan configuration used here is a line scan, which has several advantages. The different wavelengths are acquired simultaneously, as such limiting the influence of sample movement, the signal-to-noise ratio is high enabling rather short exposure times, and only a line light source is necessary (Arngren 2011; Williams 2009; Hyvärinen et al. 2008). Scanned data were corrected to cover most of the issues regarding the calibration of the NIR system. Lens effects are corrected for by use of a transformation matrix based on a scan of a grid of squares, and the images were corrected for fluctuating intensity during scanning and noise filtering as well. In almost all cases, spectral pre-treatment is a crucial step before proper models can be built. However, Liu et al. (2010) stated that the capability of spectral pre-treatment is limited. The effect of implementing more advanced methods such as extended multiplicative scatter correction (EMSC) is therefore not evaluated for the data of this article and is also beyond the proof-of-concept objective of the platform illustrated here. Future optimization could include pixel-by-pixel correction to compensate for nonlinear response of each pixel to changing reflectance (Geladi et al. 2004). In this study, scanning and processing the data took ca. 20 min per disk, although this depends on the size of the disks. It should be noted that the newest infrared cameras can even acquire spectral information of a full image at once and will enable even faster characterization.

Linking the measured characteristics, such as chemical composition, with the infrared spectra is the final aim of NIR scanning. In case of lignin, analytical pyrolysis, which only needs 75–80 µg per sample, can be used for modeling (Alves et al. 2011), thereby allowing calibration with data from the small drill hole locations on the scans for high-resolution mapping. The most straightforward approach is to select the determining wavelengths, for example by principal component analysis (PCA) followed by the use of ratio images. This is exemplified in Li et al. (2012) for citrus canker. The specific selection of a certain wavelength range can also be useful for redundancy analysis (Hedrick et al. 2007). The PLS method used in this paper is more complex, but still the most standard procedure of a wide range of available chemometric methods (Wold et al. 2001; Via et al. 2014). Chen et al. (2010) have already concluded that Fourier transform infrared (FTIR) spectroscopy coupled to chemometrics can be used for the qualitative and quantitative analysis of wood samples. Clipping the outermost wavelength bands as well as those wavelength bands determined by water for the lignin model led to small improvements in the models. R^2 and RMSE in combination with the fitted versus observed value curves of the validation data were evaluated for different models varying in the wavelength intervals accounted for and the number of

components. The number of PLS components is a crucial factor affecting the accuracy of the model, as too many components would lead to over-fitting, while too few would result in the loss of useful information (Kelley et al. 2004). The objective way to determine the number of components in this study was to calculate at which number of components the curvature of the R^2 versus number of components curve was maximized. Other calibration techniques for chemometrics that have been developed in recent years are probably of use as well (Brinkmann et al. 2002; Lestander and Rhen 2005; Mora and Schimleck 2010; Fang et al. 2011), but are beyond the scope of the proof-of-concept objective of this paper. A larger calibration set of accurate measurements will be important to optimize the models in the future, yet the 2D mapping approach is proven to be very valuable. It is possible to use the drilled holes as landmark points to align the images of different imaging modalities to be able to extract more data apart from the specific drill holes, but exactly on the same locations for all different imaging modalities. Figure 8 illustrates that more calibration data from poplar with lower density and with lower lignin content are needed to improve the current models. Furthermore, using an existing model on samples of a new site is not evident (Schimleck 2008) and rather high prediction errors when estimating glucan, xylan, cellulose and lignin contents with intact radial strips of wood by NIR can also be the result of the diverse origins of the samples (Schimleck et al. 2006).

Differences between disk averages determined by wet analysis and by NIR hyperspectral imaging (Table 3) show that the link between these averages is not straightforward. Future research needs to identify the shortcomings and their importance of both methods. Figure 7 proves that variability within as well as between wood disks can be investigated with NIR. The denser zones coincide with the tension wood zones and zones with a lower lignin content. From an anatomical point of view, tension wood zones have cells with thicker cell walls containing a G-layer. Only with recent techniques, one is able to detect the very small lignin contents in that G-layer (Joseleau et al. 2004). Mapping the tension wood zones and density variation within disks is example of how such a tool chain can contribute to strength and stability assessment of wood. Species or clones that have wood with a rather uniform density distribution and smaller tension wood zones evenly distributed across the stem are preferred for material uses. Such trees have less internal stresses, stresses that can lead to defects when dried and sawn (De Boever et al. 2011). Comprehensive decision support tools dealing with economic and silvicultural aspects of forest biomass utilization (i.a. Pasanen et al. 2008) can also benefit from data generated by this tool chain concerning the variability between disks, and by extension trees, clones or species. Correlations between various parameters as illustrated in Fig. 7 profit from the combination of various imaging techniques performed on one and the same disk which makes the investigation on a smaller, more detailed level possible. By using poplar as an exemplary wood species, proper model verification for tension wood mapping is possible. NIR-based tension wood zones correlate more with zones with different shiny appearance than with the resulting scans after tension wood coloring. This concurs with what is reported by Badia et al. (2005) using zinc-chloro-iodine coloring solutions. The technique can also be used for tension wood mapping of other species without

shininess difference, but only if there is another way to calibrate the model with spectra of tension wood and normal wood of those species, for example by usage of coloring methods, wet chemistry data or microscopic wood anatomy (Ritter et al. 1993).

The high-throughput character of the tool chain enables to generate large datasets for different research disciplines. One can obtain data in the visual, NIR and X-ray spectrum in less than 30 min, depending on the used hardware and the potential of batch scanning. Preprocessing and applying the models takes only a few minutes. This is why this high-throughput chain has potential for fast screening, for example, of young breeding material. When low resolution is acceptable, mapping is possible without the need for X-ray CT or time-consuming analyses that alter or even destroy the samples such as wet analysis and tension wood coloring. NIR-based density mapping is very similar to the X-ray density images, yet lower density regions are less accurately predicted. Although the resolution of the NIR images is lower, small distinctive zones are still visible.

Conclusion

The tool chain presented in this paper uses flatbed, X-ray and NIR scanning for mapping physical and chemical wood properties. Flatbed scanning is a simple technique providing general parameters such as shape and size of the disks, heartwood, etc. With additional weighing, green moisture content and basic density can be assessed. X-ray scans can be used for microdensitometry, and NIR spectra were used for 2D tension wood and lignin mapping. NIR scans can also be used for densitometry, if a lower resolution is sufficient or if an X-ray system is not available.

The potential of the tool chain to map various wood properties without the need for labor-intensive and sometimes difficult-to-interpret methods is proven. The benefits of such a tool chain are multiple. The resulted mapping allows to illustrate the variability of wood parameters within as well as between disks, which is interesting i.a. for tree breeders and wood processing industry. Furthermore, various properties can be assessed on one and the same disk, which is relevant for correlation studies. Future developments can focus on seamless integration of X-ray CT, NIR, optical imaging as well as imaging in other wavelength ranges to complement the techniques used in this paper. Finally, conclusions can be drawn on large sample sets thanks to the high-throughput approach.

Additional data collection in a broad spectrum database will improve the models in the future. Furthermore, it would be interesting to apply the tool chain on other tree species, but also on panels, beams or cores.

References

Alves A, Simoes R, Stackpole DJ, Vaillancourt RE, Potts BM, Schwanninger M, Rodrigues J (2011) Determination of the syringyl/guaiacyl ratio of *Eucalyptus globulus* wood lignin by near infrared-based partial least squares regression models using analytical pyrolysis as the reference method. J Near Infrared Spec 19:343–348

Arngren M (2011) Hyperspectral NIR camera. Technical University of Denmark, Kongens Lyngby. http://www2.imm.dtu.dk/pubdb/public/allpublications.php?year=2011&pubtype=6. Accessed 13 Jul 2015

Aylott MJ, Casella E, Tubby I, Street NR, Smith P, Taylor G (2008) Yield and spatial supply of bioenergy poplar and willow short-rotation coppice in the UK. New Phytol 178:358–370

Badia MA, Mothe F, Constant T, Nepveu G (2005) Assessment of tension wood detection based on shiny appearance for three poplar cultivars. Ann For Sci 62(1):43–49

Bahng MK, Mukarakate C, Robichaud DJ, Nimlos MR (2009) Current technologies for analysis of biomass thermochemical processing: a review. Anal Chim Acta 651(2):117–138

Blankenhorn PR, Bowersox TW, Strauss CH, Kessler KR, Stover LR, Kilmer WR, Dicola ML (1992) Effects of management strategy and site on specific-gravity of a *Populus* hybrid clone. Wood Fiber Sci 24(3):274–279

Boerjan W, Ralph J, Baucher M (2003) Lignin biosynthesis. Annu Rev Plant Biol 54:519–546

Brabant L, Vlassenbroeck J, De Witte Y, Cnudde V, Boone MN, Dewanckele J, Van Hoorebeke L (2011) Three-dimensional analysis of high-resolution X-ray computed tomography data with Morpho+. Microsc Microanal 17(2):252–263

Brereton NJB, Pitre FE, Ray MJ, Karp A, Murphy RJ (2011) Investigation of tension wood formation and 2,6-dichlorbenzonitrile application in short rotation coppice willow composition and enzymatic saccharification. Biotechnol Biofuels 4:13

Brereton NJB, Ray MJ, Shield I, Martin P, Karp A, Murphy RJ (2012) Reaction wood—a key cause of variation in cell wall recalcitrance in willow. Biotechnol Biofuels 5:83

Brinkmann K, Blaschke L, Polle A (2002) Comparison of different methods for lignin determination as a basis for calibration of near-infrared reflectance spectroscopy and implications of lignoproteins. J Chem Ecol 28(12):2483–2501

Chen H, Ferrari C, Angiuli M, Yao J, Raspi C, Bramanti E (2010) Qualitative and quantitative analysis of wood samples by Fourier transform infrared spectroscopy and multivariate analysis. Carbohyd Polym 82:772–778

De Boever L, Vansteenkiste D, Stevens M, Van Acker J (2011) Kiln drying of poplar wood at low temperature: beam distortions in relation to wood density, tension wood occurrence and moisture distribution. Wood Res 56(2):245–256

De Mil T, Vannoppen A, Beeckman H, Van Acker J, Van den Bulcke J (2016) A field-to-desktop toolchain for X-ray CT densitometry enables tree ring analysis. Ann Bot 117(7):1187–1196

De Ridder M, Van den Bulcke J, Vansteenkiste D, Van Loo D, Dierick M, Masschaele B, De Witte Y, Mannes D, Lehmann E, Beeckman H, Van Hoorebeke L, Van Acker J (2011) High-resolution proxies for wood density variations in *Terminalia superba*. Ann Bot-London 107(2):293–302

Defo M, Goodison A, Uy N (2009) A method to map within-tree distribution of fibre properties using SilviScan-3 data. For Chron 85(3):409–414

Dierick M, Van Loo D, Masschaele B, Boone M, Van Hoorebeke L (2010) A LabVIEW® based generic CT scanner control software platform. J X-Ray Sci Technol 18(4):451–461

Dierick M, Van Loo D, Masschaele B, Van den Bulcke J, Van Acker J, Cnudde V, Van Hoorebeke L (2014) Recent micro-CT scanner developments at UGCT. Nucl Instrum Meth B 324:35–40

Fang Y, Park JI, Jeong YS, Jeong MK, Baek SH, Cho HW (2011) Enhanced predictions of wood properties using hybrid models of PCR and PLS with high-dimensional NIR spectral data. Ann Oper Res 190(1):3–15

FAOSTAT (2013) World roundwood production. http://faostat3.fao.org. Accessed 14 Jul 2015

Freyburger C, Longuetaud F, Mothe F, Constant T, Leban JM (2009) Measuring wood density by means of X-ray computer tomography. Ann For Sci 66(8):804p1–804p9

Fujimoto T, Kurata Y, Matsumoto K, Tsuchikawa S (2008) Application of near infrared spectroscopy for estimating wood mechanical properties of small clear and full length lumber specimens. J Near Infrared Spectrosc 16(6):529–537

Fujimoto T, Kurata Y, Matsumoto K, Tsuchikawa S (2010) Feasibility of near-infrared spectroscopy for online multiple trait assessment of sawn lumber. J Wood Sci 56(6):452–459

Geladi P, Burger J, Lestander T (2004) Hyperspectral imaging: calibration problems and solutions. Chemom Intell Lab 72(2):209–217

Geyer WA, DeWyke J, Walawender WP (2000) Biomass and gasification properties of young *Populus* clones. Wood Fiber Sci 32(3):375–384

Gowen AA, O'Donnell CP, Cullen PJ, Downey G, Frias JM (2007) Hyperspectral imaging—an emerging process analytical tool for food quality and safety control. Trends Food Sci Tech 18(12):590–598

Grayson M (2011) Biofuels. Nature 474(7352 Suppl.):S1

Guidi W, Piccioni E, Ginanni M, Bonari E (2008) Bark content estimation in poplar (*Populus deltoides* L.) short-rotation coppice in Central Italy. Biomass Bioenerg 32:518–524

Hackenberg J, Wassenberg M, Spiecker H, Sun D (2015) Non destructive method for biomass prediction combining TLS derived tree volume and wood density. Forests 6(4):1274–1300

Harfouche A, Meilan R, Kirst M, Morgante M, Boerjan W, Sabatti M, Mugnozza GS (2012) Accelerating the domestication of forest trees in a changing world. Trends Plant Sci 17(2):64–72

Headlee WL, Zalesny RS, Hall RB, Bauer EO, Bender B, Birr BA, Miller RO, Randall JA, Wiese AH (2013) Specific gravity of hybrid poplars in the North-central region, USA: within-tree variability and site x genotype effects. Forests 4(2):251–269

Hedrick SE II, Bennet RM, Rials TG, Kelley SS (2007) Correlation of near-infrared spectroscopy measurements with the properties of treated wood. J Mater Civil Eng 19(4):279–285

Hein PRG, Campos ACM, Mendes RF, Mendes LM, Chaix G (2011) Estimation of physical and mechanical properties of agro-based particleboards by near infrared spectroscopy. Eur J Wood Prod 69(3):431–442

Hinchee M, Rottmann W, Mullinax L, Zhang CS, Chang SJ, Cunningham M, Pearson L, Nehra N (2009) Short-rotation woody crops for bioenergy and biofuels applications. Vitro Cell Dev-Pl 45(6):619–629

Hou S, Li LG (2011) Rapid characterization of woody biomass digestibility and chemical composition using near-infrared spectroscopy. J Integr Plant Biol 53(2):166–175

Hyvärinen T, Herrala E, Jussila J (2008) High speed hyperspectral chemical imaging. In: International near-infrared conference, Umeå, Sweden, p 6

Jones PD, Schimleck LR, Peter GF, Daniels RF, Clark A (2006) Nondestructive estimation of wood chemical composition of sections of radial wood strips by diffuse reflectance near infrared spectroscopy. Wood Sci Technol 40(8):709–720

Joseleau J, Imai T, Kuroda K, Ruel K (2004) Detection in situ and characterization of lignin in the G-layer of tension wood fibres of *Populus deltoids*. Planta 219(2):338–345

Kelley SS, Rials TG, Snell R, Groom LH, Sluiter A (2004) Use of near infrared spectroscopy to measure the chemical and mechanical properties of solid wood. Wood Sci Technol 38(4):257–276

Kenney WA, Sennerbyforsse L, Layton PA (1990) Review of biomass quality research relevant to the use of poplar and willow for energy-conversion. Biomass 21(3):163–188

León K, Mery D, Pedreschi F, León J (2006) Color measurement in L*a*b* units from RGB digital images. Food Res Int 39(10):1084–1091

Lestander TA, Rhen C (2005) Multivariate NIR spectroscopy models for moisture, ash and calorific content in biofuels using bi-orthogonal partial least squares regression. Analyst 130(8):1182–1189

Li J, Rao X, Ying Y (2012) Development of algorithms for detecting citrus canker based on hyperspectral reflectance imaging. J Sci Food Agric 92:125–134

Li WZ, Van den Bulcke J, De Windt I, Van Loo D, Dierick M, Brabant L, Van Acker J (2013) Combining electrical resistance and 3-D X-ray computed tomography for moisture distribution measurements in wood products exposed in dynamic moisture conditions. Build Environ 67:250–259

Liu L, Ye XP, Saxton AM, Womac A (2010) Pretreatment of near infrared spectral data in fast biomass analysis. J Near Infrared Spectrosc 18(5):317–331

Mayo SC, Chen F, Evans R (2010) Micron-scale 3D imaging of wood and plant microstructure using high-resolution X-ray phase-contrast microtomography. J Struct Biol 171(2):182–188

McKendry P (2002) Energy production from biomass (part 1): overview of biomass. Bioresour Technol 83(1):37–46

Meder R, Marston D, Ebdon N, Evans R (2010) Spatially-resolved radial scanning of tree increment cores for near infrared prediction of microfibril angle and chemical composition. J Near Infrared Spectrosc 18(3):499–505

Mézáros E, Jakab E, Vàrhegyi G, Szepesváry P, Mirosvölgyi B (2004) Comparative study of the thermal behaviour of wood and bark of young shoots obtained from an energy plantation. J Anal Appl Pyrolysis 72:317–328

Mora CR, Schimleck LR (2010) Kernel regression methods for the prediction of wood properties of *Pinus taeda* using near infrared spectroscopy. Wood Sci Technol 44(1):561–578

Mora CR, Schimleck LR, Yoon SC, Thai CN (2011) Determination of basic density and moisture content of loblolly pine wood disks using a near infrared hyperspectral imaging system. J Near Infrared Spectrosc 19(5):401–409

Murphey WK, Bowersox TW, Blankenhorn PR (1979) Selected wood properties of young *Populus* hybrids. Wood Sci 11(4):263–267

Nkansah K, Dawson-Andoh B (2010a) Rapid characterization of biomass using fluorescence spectroscopy coupled with multivariate data analysis. I. Yellow poplar (*Liriodendron tulipifera* L.). J Renew Sustain Ener. 2(2):023103

Nkansah K, Dawson-Andoh B (2010b) Rapid characterization of biomass using fluorescence spectroscopy coupled with multivariate data analysis. II. Northern red oak (*Quercus rubra*). J Renew Sustain Ener 2(4):043101

Pasanen K, Stupak I, Röser D, Asikainen A, Raulund Rasmussen K (2008) Enertree—Decision support tool to analyse forest biomass extraction scenarios. In: Röser D, Asikainen A, Raulund-Rasmussen K, Stupak I (eds) Sustainable Use of Forest Biomass for Energy: a synthesis with focus on the Baltic and Nordic Region. Springer, Berlin, pp 235–255

Poke FS, Raymond CA (2006) Predicting extractives, lignin, and cellulose contents using near infrared spectroscopy on solid wood in *Eucalyptus globulus*. J Wood Chem Technol 26(2):187–199

Polle A, Eiblmeier M, Sheppard L, Murray M (1997) Responses of antioxidative enzymes to elevated CO_2 in leaves of beech (*Fagus sylvatica* L.) seedlings grown under a range of nutrient regimes. Plant Cell Environ 20(10):1317–1321

Rae A, Street N, Robinson K, Harris N, Taylor G (2009) Five QTL hotspots for yield in short rotation coppice bioenergy poplar: the poplar biomass loci. BMC Plant Biol 9:23

Raymond CA, Schimleck LR (2002) Development of near infrared reflectance analysis calibrations for estimating genetic parameters for cellulose content in *Eucalyptus globulus*. Can J For Res 32(1):170–176

Riddell M, Cown D, Harrington J, Lee J, Moore J (2012) Assessing spiral grain angle by light transmission—Proof of concept. IAWA J 33(1):1–14

Ritter DC, Kroll RE, Gertjejansen RO (1993) Zones of gelatinous fibers in *Populus balsamifera* L. Wood Fiber Sci 25(2):198–208

Santos AJA, Anjos O, Simões R, Rodrigues J, Pereira H (2014) Kappa number prediction of *Acacia melanoxylon* unbleached kraft pulps using NIR-PLSR models with a narrow interval of variation. BioResources 9(4):6735–6744

Santos AJA, Anjos O, Pereira H (2015) Estimation of *Acacia melanoxylon* unbleached kraft pulp brightness by NIR spectroscopy. Forest Syst. 24(2):wRC03–wRC06

Schimleck LR (2008) Near-infrared spectroscopy: a rapid non-destructive method for measuring wood properties, and its application to tree breeding. New Zeal J For Sci 38(1):14–35

Schimleck LR, Evans R, Ilic J (2001) Estimation of *Eucalyptus delegatensis* wood properties by near infrared spectroscopy. Can J For Res 31(10):1671–1675

Schimleck LR, Evans R, Matheson AC (2002) Estimation of *Pinus radiata* D. Don clear wood properties by near-infrared spectroscopy. J Wood Sci 48:132–137

Schimleck LR, Downes GM, Evans R (2006) Estimation of *Eucalyptus nitens* wood properties by near infrared spectroscopy. Appita J 59(2):136–141

Schinker MG, Hansen N, Spiecker H (2003) High-frequency densitometry—a new method for the rapid evaluation of-wood density variations. IAWA J 24(3):231–239

Schwanninger M, Rodrigues JC, Fackler K (2011) A review of band assignments in near infrared spectra of wood and wood components. J Near Infrared Spectrosc 19(5):287–308

Semen E, Kuo ML, Su YC, Hall RB, Stokke DD (2001) Physical properties of kraft pulp from four-year-old aspen hybrids and crosses. Wood Fiber Sci 33(1):140–147

Skog J, Oja J (2009) Heartwood diameter measurements in *Pinus sylvestris* sawlogs combining X-ray and three-dimensional scanning. Scand J For Res 24(2):182–188

So CL, Via BK, Groom LH, Schimleck LR, Shupe TF, Kelley SS, Rials TG (2004) Near infrared spectroscopy in the forest products industry. For Prod J 54(3):6–16

Tharakan PJ, Volk TA, Abrahamson LP, White EH (2003) Energy feedstock characteristics of willow and hybrid poplar clones at harvest age. Biomass Bioenerg 25:571–580

Thumm A, Riddell M, Nanayakkara B, Harrington J, Meder R (2010) Near infrared hyperspectral imaging applied to mapping chemical composition in wood samples. J Near Infrared Spectrosc 18(6):507–515

Timell TE (1969) Chemical composition of tension wood. Sven Papp 72(6):173–181

Tsuchikawa S (2007) A review of recent near infrared research for wood and paper. Appl Spectrosc Rev 42(1):43–71

Tsuchikawa S, Kobori H (2015) A review of recent application of near infrared spectroscopy to wood science and technology. J Wood Sci 61:213–220

Tsuchikawa S, Schwanninger M (2013) A review of recent near-infrared research for wood and paper (Part 2). Appl Spectrosc Rev 48(7):560–587

Vahey DW, Zhu JY, Scott CT (2007) Wood density and anatomical properties in suppressed-growth trees: comparison of two methods. Wood Fiber Sci 39(3):462–471

Van den Bulcke J, Masschaele B, Dierick M, Van Acker J, Stevens M, Van Hoorebeke L (2008) Three-dimensional imaging and analysis of infested coated wood with X-ray submicron CT. Int Biodeter Biodegr 61(3):278–286

Van den Bulcke J, De Boever L, De Vetter L, Van Acker J, Verheyen K (2013) A low-cost tool-chain for reconstruction of standing trees of selected European hardwood species. Wood Res 58(2):201–216

Van den Bulcke J, Wernersson ELG, Dierick M, Van Loo D, Masschaele B, Brabant L, Boone MN, Van Hoorebeke L, Haneca K, Brun A, Hendriks CLL, Van Acker J (2014) 3D tree-ring analysis using helical X-ray tomography. Dendrochronologia 32(1):39–46

Verlinden MS, Broeckx LS, Van den Bulcke J, Van Acker J, Ceulemans R (2013) Comparative study of biomass determinants of 12 poplar (*Populus*) genotypes in a high-density short-rotation culture. For Ecol Manag 307:101–111

Via BK, Zhou CF, Acquah G, Jiang W, Eckhardt L (2014) Near Infrared Spectroscopy Calibration for Wood Chemistry: which Chemometric Technique Is Best for Prediction and Interpretation? Sensors 14(8):13532–13547

Vlassenbroeck J, Dierick M, Masschaele B, Cnudde V, Hoorebeke L, Jacobs P (2007) Software tools for quantification of X-ray microtomography. Nucl Instrum Meth A 580(1):442–445

Wassenberg M, Montwé D, Kahle H-P, Spiecker H (2014) Exploring high frequency densitometry calibration functions for different tree species. Dendrochronologia 32(3):273–281

Whetten RW, MacKay JJ, Sederoff RR (1998) Recent advances in understanding lignin biosynthesis. Annu Rev Plant Phys 49:585–609

Williams PJ (2009) Near infrared (NIR) hyperspectral imaging for evaluation of whole maize kernels: chemometrics for exploration and classification. Dissertation, Stellenbosch University

Wold S, Trygg J, Berglund A, Antti H (2001) Some recent developments in PLS modeling. Chemom Intell Lab 58(2):131–150

Wyman CE (2007) What is (and is not) vital to advancing cellulosic ethanol. Trends Biotechnol 25(4):153–157

Zhou GW, Taylor G, Polle A (2011) AFTIR-ATR-based prediction and modelling of lignin and energy contents reveals independent intra-specific variation of these traits in bioenergy poplars. Plants Methods 7:9

Zhu JY, Scott CT, Scallon KL, Myers GC (2007) Effects of plantation density on wood density and anatomical properties of red pine (*Pinus resinosa* Ait.). Wood Fiber Sci 39(3):502–512